Available online at www.sciencedirect.com
SCIENCE DIRECT®
Journal of Catalysis 221 (2004) 127–136
JOURNAL OF CATALYSIS
www.elsevier.com/locate/jcat

Effect of crystal size on the oxidative dehydrogenation of butane on V/MgO catalysts

R. Vidal-Michel and K.L. Hohn *

Department of Chemical Engineering, Kansas State University, Manhattan, KS 66506, USA

Received 5 May 2003; revised 14 July 2003; accepted 16 July 2003

Abstract

Producing metal oxide catalysts with nanometer crystal sizes offers an attractive means of controlling catalytic behavior in selective oxidation reactions. In this work, the catalytic behavior of MgO nanocrystal-supported vanadium was compared to that of vanadium supported on conventionally prepared MgO. It was found that nanocrystals gave higher butene selectivity for weight loadings of 5, 15, and 25%, producing less CO, ethylene, and propylene. Both types of catalysts were characterized using nitrogen adsorption, Raman spectroscopy, XRD, TEM, and XANES to determine the structure of vanadium on the magnesium oxide surface. The catalyst surface structure appears to be similar on both types of catalysts, with a magnesium orthovanadate phase supported on a MgO phase. It is hypothesized that the chemical nature of the support, specifically acid/base properties, was responsible for the differences noted in catalytic behavior, though differences in the domain size of $Mg_3(VO_4)_2$ could also play a role.

Keywords: Oxidative dehydrogenation; Butane; Vanadium; Nanoscale catalysts; Selective oxidation

1. Introduction

Manipulating catalytic material dimensions at the nanometer scale presents a fascinating avenue for producing more active and selective catalysts. Within the last 10 years a number of authors have synthesized metal oxides with crystal sizes of 1–10 mm for use as catalytic materials. Tschope and Ying used inert gas condensation to prepare more active nanoscale CeO_2 for the reduction of SO_2 by CO [1]. Photocatalytic oxidation on nanoscale TiO_2 has been reported by a number of authors [2–4]. Palmqvist and co-workers have prepared nanoscale doped and undoped CeO_2 for use as catalysts for the total oxidation of methane [5] and the reduction of SO_2 by CO [6]. Yoo reported on the use of oxide nanoparticles for selective gas-phase oxidation of *p*-xylene and oxidative dehydrogenation of alkanes [7]. Pak and coworkers studied vanadium supported on MgO nanocrystals for propane oxidative dehydrogenation [8], while Chesnokov and co-workers used similar catalysts for butane oxidative dehydrogenation [9].

Most of these studies focused on environmental applications, where the primary purpose of the nanoscale metal oxide was to store and transport oxygen. It is clear from the literature that nanoscale metal oxides can be highly active in these applications. It is less clear whether these materials can act as *selective* oxidation catalysts, where an intermediate oxidation product is desired. Pak and coworkers reported that V/MgO nanocrystals provided high reaction rates in propane oxidative dehydrogenation, but did not extensively explore selectivity differences between nanocrystals and microcrystals. Yoo suggested that *p*-xylene oxidation and oxidative dehydrogenation of lower alkanes could occur selectivity on nanosized supported metal and metal oxides prepared through CVD, but did not make a comparison with conventional materials. Chesnokov found that vanadium supported on MgO nanocrystals was active and selective in butane oxidative dehydrogenation, but made no comparison with vanadium supported on conventional MgO.

To understand whether metal oxide nanocrystals have unique properties for selective oxidation, it is critical to

* Corresponding author.
E-mail address: hohn@ksu.edu (K.L. Hohn).

0021-9517/$ – see front matter
doi:10.1016/j.jcat.2003.07.002

compare their performance with conventional metal oxides. In particular, selectivity differences are important to show whether modifying the crystal size changes the surface chemistry rather than just leading to higher surface areas. This work focuses on whether metal oxide nanocrystals have unique catalytic properties for oxidative dehydrogenation of butane. Catalytic results for vanadium supported on MgO nanocrystals prepared using a modified sol–gel synthesis and on MgO prepared using a conventional technique are compared. The surface structure of vanadium in these two catalysts is also studied in an attempt to rationalize the catalytic differences.

2. Experimental

2.1. Preparation of V/MgO catalysts

For V/MgO nanocrystals, MgO was synthesized through an aerogel method [10] using a bench-top autoclave Parr Model 4843. In a two-necked 500 mL flask, 5 g of magnesium ribbons (Alfa Aesar, 99.8% purity) was reacted with 200 mL of methanol under nitrogen. The Mg/methanol mixture was magnetically stirred 2 h or until no Mg shavings were visible. The resultant solution was a 1 M solution of $Mg(OCH_3)_2$. Hydrolysis of this solution was achieved by mixing with 200 mL of toluene and then slowly adding 4 mL of distilled water with a syringe. This mixture was stirred overnight, forming a magnesium hydroxide gel. Next the gel was dehydrated through hypercritical drying in an autoclave. The gel was placed in the autoclave, and the autoclave was pressurized to 100 psi with nitrogen. Over a 4-h period, the solution was heated from room temperature to 265 °C, which resulted in a pressure of 800 psi. This procedure produced a fine, white magnesium hydroxide powder. This powder was calcined at 500 °C under vacuum overnight.

For V/MgO microcrystals, commercially purchased MgO (Aldrich, 99 + % purity) was modified to give a higher surface area [10]. Several grams of CM MgO was boiled in 500 mL of distilled water overnight while being stirred. After cooling, the solution was filtered. A paste of magnesium hydroxide was recovered and dried in an oven at 120 °C for 2 h and then gradually heated to 500 °C under vacuum and left at that temperature overnight.

Supported vanadium nanocrystals and microcrystals were prepared using the same procedure, with the only difference being the MgO starting material. Freshly obtained MgO was impregnated with a solution of $V(acac)_3$ in THF overnight at ambient temperature with enough $V(acac)_3$ to produce samples with 5, 15, and 25 wt% vanadium oxide (V_2O_5). After filtration, the slurry was washed with pure, dry THF until the filtrate was colorless. The recovered solid was then heated to 500 °C under a flow of air and calcined at the same temperature overnight. For nanocrystals, the calcinations were done under vacuum, while for microcrystals it was done at atmospheric pressure. The resulting V/MgO powder was then pelletized in a small hydraulic press at 225 N, crushed, and sieved between 20 and 40 mesh sieves (420–850 μm). V/MgO nanocrystals prepared using the aerogel method will be referred to as AP V/MgO, while V/MgO synthesized using conventionally prepared MgO will be referred to as CP V/MgO. Weight percents discussed in this paper refer to the values calculated from the mass of the support and the vanadium salt used in preparation. No direct measurement of the V_2O_5 weight percent was made.

2.2. Catalyst characterization

Surface area measurements were conducted using a Quantachrome NOVA 1200 instrument. Approximately 0.1 g of catalyst was degassed at 150 °C for 45 min. Seven-point BET surface areas were found from the nitrogen adsorption isotherms.

X-ray powder diffraction was carried out in a Scintag XDS 2000 spectrometer. Cu-K_α radiation was the light source with applied voltage of 40 KV and current of 40 mA. Two theta angles ranged from 20 to 85° with a speed of 2° per minute. The crystallite size was calculated using the Scherrer equation.

TEM experiments were conducted by Dan Boyle at the Kansas State University Microscopy and Image Processing Facility using a Philips CM 100 TEM. Ground V/MgO powder was collected onto a carbon-coated copper grid for analysis.

Raman spectra were collected in a Nicolet Nexus 670 FTIR spectrometer with an FT-Raman attachment. The spectra were recorded using 1024 scans at 4 cm^{-1} resolution using a Germanium detector. One of the spectra (15 wt%, CP V/MgO) had a strong increasing background that obscured the relevant peaks. For this sample, a multispline fit was used to eliminate the background.

X-ray absorption spectra were collected on the BESSRC CAT station 12-BM-B at the Advanced Photon Source. The monochromator, equipped with Si (111) crystals, was calibrated by setting the inflection point of the first derivative from the V *K* edge to 5465 eV. Flourescence data were collected using a Lytle detector. Energy resolution was approximately 1 eV. All reported spectra represent the average of three trials. Repeat trials were in excellent agreement with one another. Preedge peak positions differed by no more than 0.2 eV, while the edge and the $1s \rightarrow 4p$ transition energies differed by no more than 0.4 eV. XANES spectra were analyzed by first fitting the preedge baseline with a least-squares fit and then subtracting the baseline from the spectrum. The near-edge data were normalized by dividing by the height of the linear portion of the absorption spectrum $\sim$100 eV above the absorption edge.

2.3. Catalytic activity testing

Experiments to test the catalytic activity of all samples were performed in an 11-mm i.d. quartz tube reactor placed

inside a cylindrical furnace. One gram of catalyst was placed between plugs of quartz wool. Two type K thermocouples were placed at the front and back of the catalyst bed. Since high conversions were achieved in most experiments, the bed was not completely isothermal. The temperature difference was less than 10 °C between the front and the back in all experiments. The inlet temperature is used as the reaction temperature.

Butane (99.0%) and oxygen (grade 4.4) were obtained from Linweld. Nitrogen (97.0 + %) was obtained from Airgas. All gases were used without further purification. Gas flow rates were regulated by mass flow controllers (Unit Instruments Inc. Model 7300). Products were analyzed using a gas chromatograph (SRI 8610) equipped with MolSieve 5A and HaySep D columns and flame ionization and thermal conductivity detectors. Products detected include oxygen, carbon monoxide, carbon dioxide, methane, ethane, ethylene, propane, propylene, *n*-butane, butene, and pentane. The gas chromatograph was unable to resolve isomers of butene, so the total butene selectivity (1-butene + 2-butene) is reported. Butadiene was not detected under any condition. Water was not analyzed; instead, the moles of water produced were determined from the oxygen balance. Reported selectivities are molar selectivities.

Total gas flow was 0.5 standard liters per minute (SLPM), with 88% nitrogen dilution and a fuel/O_2 ratio equal to one-half. Reaction temperature was 500 °C and reaction pressure was 2 psig. Nitrogen was flowed to start while the inlet temperature was raised to its reaction value. Fuel and oxygen were then added to the gas flow to initiate reaction. Their addition to the gas flow was responsible for a slight drop of the inlet temperature, and 20 min were necessary to let the temperature go back up to the desired reaction value. Samples of gas flow were then analyzed every 50 min for 10 to 12 h. For CP V/MgO samples, an activation period was noted. Reported results for CP V/MgO catalysts represent steady-state results, achieved after 8 h.

To assess the possible contribution of homogeneous chemistry, reaction was carried out as described above in the absence of catalysts. Fuel and oxygen conversions were less than 1% in these experiments, indicating a negligible contribution of homogeneous chemistry.

Carbon and hydrogen mass balances closed within 10%, most within 5%. Multiple trials for each catalyst were conducted to estimate the error in the measurements and to determine whether catalyst activation was important. In general, repeat trials had butane conversions within 5% while major product selectivities agreed within 3%. In addition, two samples each for 15% V/MgO nanocrystals and microcrystals were run to estimate the experimental differences between different samples. The standard deviations of these repeat trials were used to estimate the 95% confidence intervals for the measured conversions and selectivities.

3. Results

3.1. Surface area analysis

The surface areas of 5, 15, and 25 wt% V/MgO catalysts for both the AP and CP MgO supports are shown in Table 1. As shown in this table, surface area generally decreases as the vanadium loading is increased, with the exception of a V_2O_5 weight loading of 15% for the CP V/MgO, which is slightly higher than that at 5 wt%. These results agree qualitatively with previous researchers who found the surface area decreased with weight loading for V/MgO catalysts prepared from NH_4VO_3 [11,12] and OV $(O^tBu)_3$ [8].

3.2. X-ray diffraction

X-ray diffraction results for nanocrystals (Fig. 1A) and microcrystals (Fig. 1B) as functions of vanadium weight percent are shown in Fig. 1. Irrespective of which crystal size was studied or what the weight loading of vanadium was, the only detectable peaks are at 43 and 62°. These peaks are characteristic of MgO. There may be some features between 30 and 40°, corresponding to magnesium orthovanadate [9,13,14], but these features are not distinct enough for analysis. This suggests that if vanadium-containing phases are present, they are small and poorly crystalline. This is in agreement with Chaar and co-workers [11] and Pak and co-workers [8] who did not detect clear vanadium-containing peaks for V_2O_5 weight loadings below 30%, although Chesnokov and co-workers detected peaks at 35.5 and 38° for their V/MgO catalysts prepared using a similar procedure to this work [9].

The diffraction peaks for AP V/MgO are broader than those for CP V/MgO, confirming that the crystal size is smaller for these materials. Using the peak width at 43°, the crystal sizes of the different catalysts were estimated and are reported in Table 1. The crystal size for AP V/MgO increases from 3.9 to 5.2 nm as the weight loading increases from 5 to 15 wt%. There is no clear trend in crystal size for the microcrystals, as crystal size at 15% is smaller than 5% while 25% is larger than 5%. However, for all weight loadings, the crystal size of CP V/MgO is larger than that for AP V/MgO.

3.3. Transmision electron micrographs

Fig. 2 shows the transmission electron micrograph for CP 15% V/MgO at 46,000 times magnification, while

Table 1
Surface areas and crystal sizes for AP and CP V/MgO

wt%	AP V/MgO		CP V/MgO	
	Crystal size (nm)	Surface area (m^2/g)	Crystal size (nm)	Surface area (m^2/g)
5	3.9	302.8	8.0	107.3
15	4.7	199.9	6.9	113.4
25	5.2	141.0	8.2	65.9

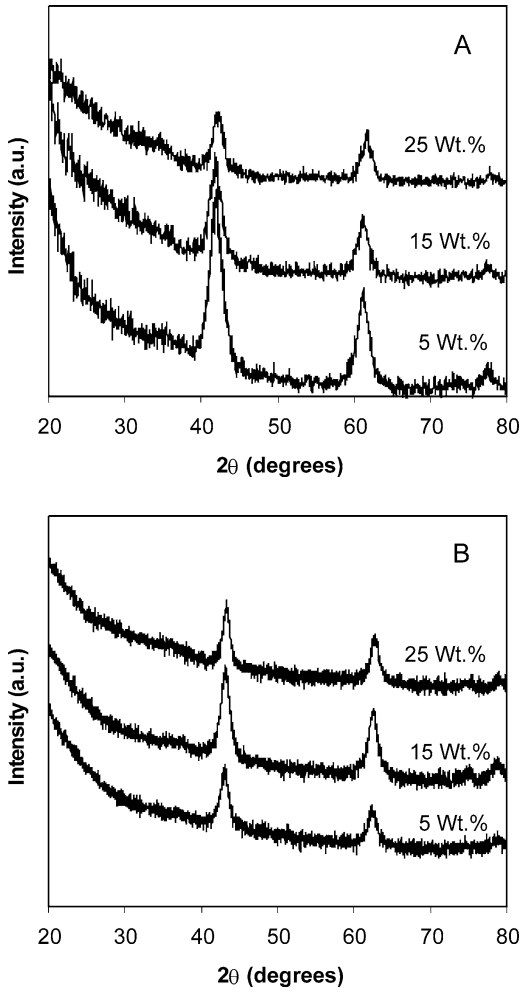

Fig. 1. Powder X-ray diffraction patterns for AP V/MgO (A) and CP V/MgO (B) with different V_2O_5 weight loadings.

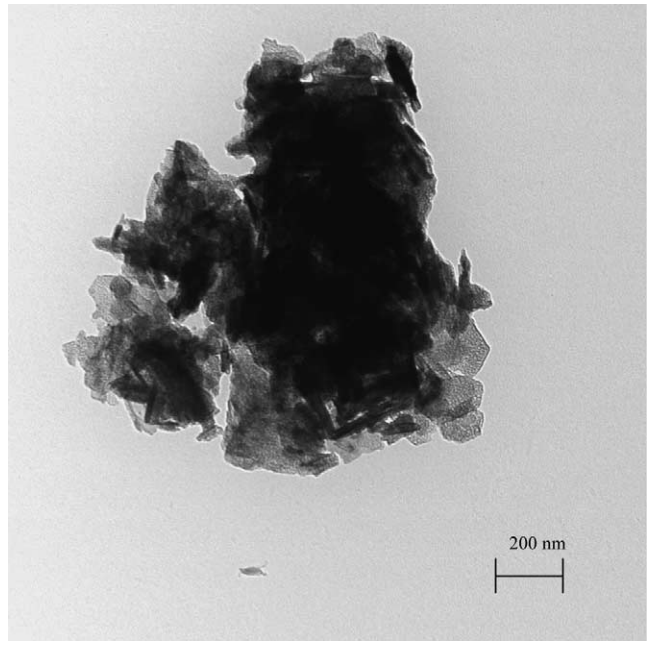

Fig. 2. Transmission electron micrograph of 15 wt% CP V/MgO, 4600 times magnification.

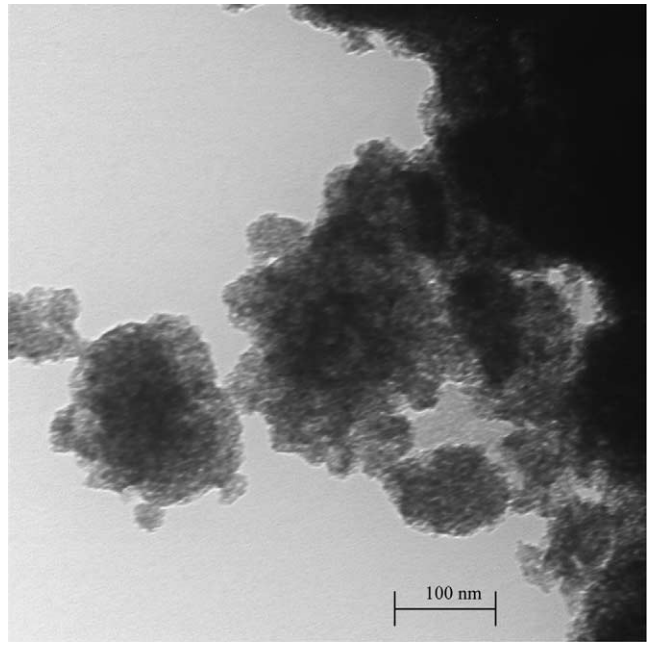

Fig. 3. Transmission electron micrograph of 15 wt% AP V/MgO, 130,000 times magnification.

Fig. 3 shows the TEM micrograph for AP 15% V/MgO at 130,000 times magnification. Fig. 4 is a more magnified view (245,000 times) of AP V/MgO. The micrographs show large differences in morphology between the two samples. The CP sample has large hexagonal MgO platelets. There are a number of darkened needle-like features on top of the hexagonal platelets. The darkness indicates the presence of vanadium due to its greater electron density than magnesium. The AP samples, on the other hand, are composed of numerous small (< 10 mm) features. These appear to be individual nanometer-sized crystallites. Again, the darker features indicate the present of vanadium. The edges of the nanocrystals appear to be quite rough, in contrast to the many smooth edges apparent on the CP V/MgO sample.

The crystal size distribution for AP 15% V/MgO was estimated from the transmission electron micrograph by measuring the sizes of 100 of the nanometer-sized features. Fig. 5 shows the distribution of crystal sizes. The crystal size distribution is skewed to the right, with the maximum frequency occurring between 4 and 6 nm. Nearly 50% of all crystallites are in this range This is in agreement with the average crystal size calculated by XRD peak broadening. However, 25% of all crystals have sizes between 6 and 8 nm and 21% have sizes in excess of 8 nm. Since the actual crystal lattice could not be distinguished in the TEM micrograph, it is not clear whether these features actually represent one or many crystallites.

It was not possible to calculate the crystal size distribution for CP V/MgO since individual crystallites could not

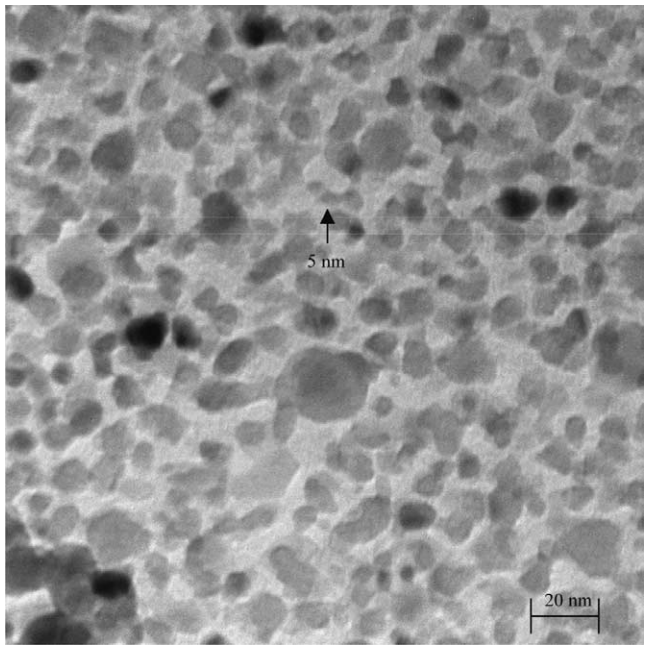

Fig. 4. Transmission electron micrograph of 15 wt% AP V/MgO, 450,000 times magnification.

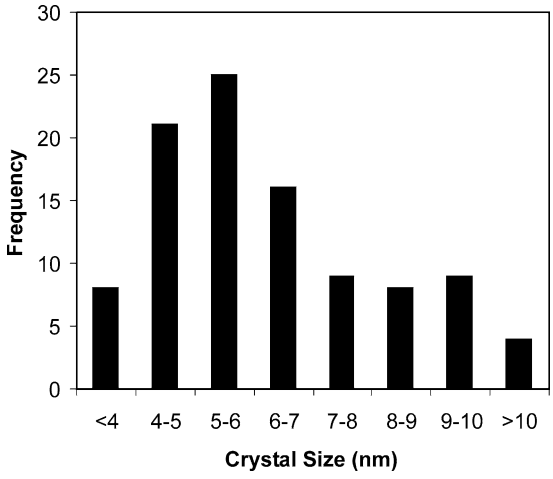

Fig. 5. Histogram of crystal size on 15 wt% AP V/MgO obtained by measuring the crystal sizes of 100 crystallites in Fig. 4.

be discerned. However, a high-resolution TEM micrograph of CP MgO reported in the literature [10] was used to estimate the crystal size distribution of CP MgO. The MgO aggregates were made up of stacked platelets, similar to that seen in Fig. 3. Measuring dimensions for 10 representative crystallites, it was found that the thickness of each platelet averaged 7.6 nm with a standard deviation of 2.2 nm and the length of the crystallite terrace averaged 13.6 nm with a standard deviation of 3.1 nm.

3.4. Raman spectroscopy

Fig. 6A shows the Raman spectra for AP V/MgO with weight loadings of 5, 10, 15, 20, and 25%. For 5% vanadium,

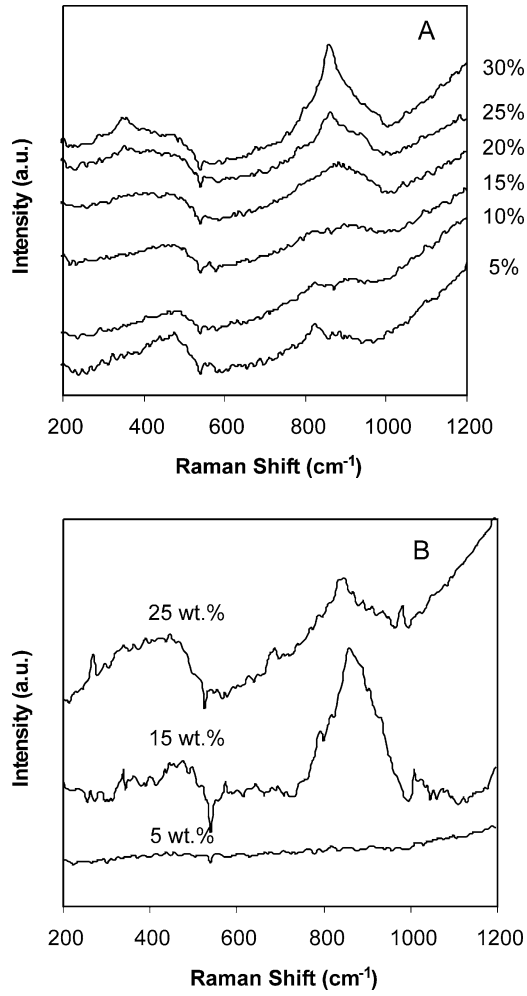

Fig. 6. Raman spectra for AP V/MgO (A) and CP V/MgO (B) with different V_2O_5 weight loadings.

there are two peaks: a broad peak at just over 400 cm^{-1}, and one at $\sim$825 cm^{-1}. The same peaks are apparent as the weight loading increases to 10 and 15%, although they are not very sharp. In addition, there is a broad feature with low intensity between 900 and 950 cm^{-1}. For 20% V/MgO, there is a broad peak between 800 and 1000 cm^{-1}, with no clear peak at 825 cm^{-1} as for the lower weight loadings. Around 400 cm^{-1} there is a broad feature with low intensity. For the highest two weight loadings, there are sharp peaks around 860 cm^{-1}, and shoulders that extend beyond 900 cm^{-1}. In the lower part of the spectra, these two samples have broad features at just under 400 cm^{-1}, with small peaks at $\sim$360 cm^{-1} on top of the broad feature. Previous studies have suggested that peaks at 380, 825, and 860 cm^{-1} result from V–O bonds stretches in magnesium orthovanadate ($Mg_3(VO_4)_2$) [8,15,16]. Therefore, the Raman results for the nanocrystals suggest that at all loadings, magnesium orthovanadate is present, and that the amount of magnesium orthovanadate increases with weight loading. Peaks at 902 and 950 cm^{-1} have been attributed to pyrovanadate ($Mg_2(V_2O_7)$) [14,16]. There is no evidence for magnesium

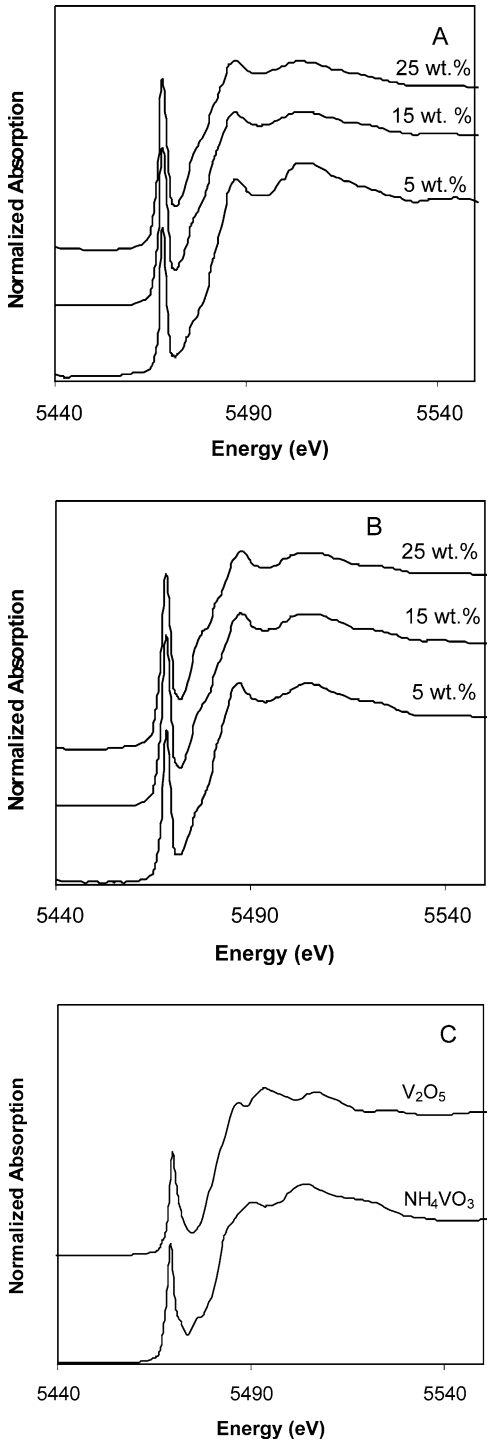

Fig. 7. XANES spectra for AP V/MgO (A), CP V/MgO (B), and V_2O_5 and NH_4VO_3 (C).

pyrovanadate for 5% V/MgO, but all other catalysts have features in the range of 900–950 cm^{-1} that may indicate the presence of magnesium pyrovanadate. It should be noted that there are no peaks at $\sim$1000 cm^{-1}, where V=O bonds should exist. This shows that there are no V_2O_5 crystallites or isolated tetrahedral vanadyl groups with terminal V=O bonds, as in the case for vanadium on supports such as Al_2O_3, SiO_2, and ZrO_2 [17]. These results agree in general with the Raman spectroscopy results of Pak and co-workers who synthesized V/MgO catalysts using MgO nanocrystals and a $OV(O^tBu)$ vanadium precursor [8].

Fig. 6B shows the Raman spectra for CP V/MgO with V_2O_5 weight loadings of 5, 15, and 25%. There are no detectable features in the 5 wt% spectrum. The spectrum for the 15 wt% sample shows a broad feature in the region of 350–500 cm^{-1}. There is a large, broad peak between 740 and 980 cm^{-1}. This peak has a shoulder at $\sim$825 cm^{-1} and a maximum at $\sim$860 cm^{-1}, indicating the presence of magnesium orthovanadate. No clear features can be seen that indicate magnesium pyrovanadate, although the peak extends into the range where magnesium pyrovanadate peaks would appear (950 cm^{-1}). For the 25% V_2O_5 spectrum, there are broad peaks at $\sim$400 cm^{-1} and between 800 and 950 cm^{-1}. These results suggest that there is magnesium orthovanadate present on the 15 and 25% samples, and possibly magnesium pyrovanadate as well. Again, there are no peaks that would suggest the presence of groups with V=O bonds.

3.5. XANES

Fig. 7 shows XANES results for AP V/MgO (Panel A) and CP V/MgO (Panel B) for different weight loadings and for two reference materials (Panel C), while Table 2 summarizes important XANES features for all catalysts and reference compounds. In all spectra, there is an intense preedge peak near 5468.4 eV. This peak has been attributed to the dipole forbidden 1s $\rightarrow$ 3d transition that is allowed due to mixing of 3d and 4p orbitals and overlap of the vanadium 3d orbitals with the 2p orbitals of neighboring oxygen [18]. As the symmetry around vanadium is lowered from octahedral to square pyramidal to tetrahedral, the molecular cage around vanadium is decreased, leading to greater mixing and overlap of orbitals and a greater intensity for the preedge peak. The preedge peaks of all catalysts have a similar intensity to that of NH_4VO_3 and much higher than that of V_2O_5, suggesting that VO_x groups in all of the V/MgO catalysts prepared in this work have a tetrahedral geometry.

Table 2
Summary of XANES results for AP and CP V/MgO catalysts and reference materials

Sample	Preedge position (eV)	Preedge peak height	Preedge peak width (eV)	1s $\rightarrow$ 4p transition
NH_4VO_3	5469.2	0.84	2.1	5491.0
V_2O_5	5469.8	0.73	2.3	5493.5
5% AP V/MgO	5468.4	0.83	1.7	5487.6
15% AP V/MgO	5468.4	0.80	2.3	5487.2
25% AP V/MgO	5468.4	0.84	2.4	5487.2
5% CP V/MgO	5468.2	0.89	2.0	5486.7
15% CP V/MgO	5468.2	0.91	2.2	5487.4
25% CP V/MgO	5468.2	0.93	2.4	5487.3

The sharpness of the preedge peak has been correlated with the spread of V–O distances [18,19]. Wong et al. found that a larger spread of the V–O distances gave broader preedge peaks in a series of tetrahedral vanadium compounds. The 1s–3d core hole Coulomb interaction changes with bond length, leading to differences in the 1s → 3d transition and, therefore, the preedge peak. The peak widths at half the maximum for all catalysts and reference materials are reported in Table 2. These widths are accurate within ±0.1 eV. It can be seen that there is a trend toward increasing peak width with increasing vanadium loading on both AP and CP MgO. The peak widths for AP and CP V/MgO are similar at weight loadings of 15 and 25%; however, the peak width of AP V/MgO is smaller than that of CP V/MgO. In addition, it can be seen that the peak widths at half height for all V/MgO catalysts, with the exception of 5 wt% AP V/MgO, are similar to that of NH_4VO_3. This suggests that the spread of V–O bond distances is similar to that of NH_4VO_3, which is known to have two V–O bonds with length of 0.181 nm and two other terminal V–O bonds of 0.166 nm [20]. The changing peak widths for V/MgO catalysts may reflect a change in the relative amounts of magnesium orthovanadate and magnesium pyrovanadate. Magnesium pyrovanadate has a range of V–O bond lengths from 0.163 to 0.182 nm [21], while the bond lengths for magnesium orthovanadate varies only between 0.17 and 0.181 nm [22]. Therefore, the increase of the peak width with vanadium oxide loading may result from an increased amount of magnesium pyrovanadate.

For all spectra, there are two peaks after the edge. The first peak, at ∼5488 eV, has been assigned to the dipole-allowed transition from 1s to the 4p level [23]. That peak and the peak at 5505 eV have previously been observed for a variety of vanadium compounds [18,24] and supported vanadium catalysts [19,25,26]. For V_2O_5 crystallites, an additional peak has been found at 5492 eV [24,27]. The absence of this peak in Fig. 3 suggests that there are no V_2O_5 crystallites on any of the V/MgO catalysts.

Comparison of the V/MgO catalysts with the reference materials shows that the preedge peak location and the 1s → 4p location are both at lower energies for the V/MgO catalysts. Tanaka and co-workers found that the energy for the 1s → 4p transition was lower for supported vanadium on alumina and silica than for bulk V_2O_5 [19]. They attributed this difference to an unknown surface vanadate. In this work, the lower 1s → 4p energy likewise indicates a surface vanadate other than V_2O_5, but here it can reasonably be concluded that the surface phase is magnesium orthovanadate and/or magnesium pyrovanadate.

3.6. Catalytic results

For all trials, oxygen conversion was complete. Fig. 8 shows butane conversion and butene selectivity for AP and CP V/MgO as functions of vanadium weight loading, along with the 95% confidence intervals. For AP V/MgO, butane conversion increases as vanadium weight loading is increased, from 52 to 60%. For CP V/MgO butane conversion is 59% at a weight loading of 5%, falls to 53% at a weight loading of 15%, before increasing to 62%. For all three weight loadings, butane conversion is slightly higher for CP V/MgO than for AP V/MgO, but the difference is within experimental error. For AP V/MgO, butene selectivity increases from 38 to 40% as weight loading is increased from 5 to 15%, but then decreases to 34%. For CP V/MgO, butene selectivity increases as weight loading is increased, going from 22% at a weight loading of 5 to 27% at a weight loading of 25%. At all weight loadings, the butene selectivity is higher on AP V/MgO than on CP V/MgO, even after considering experimental error.

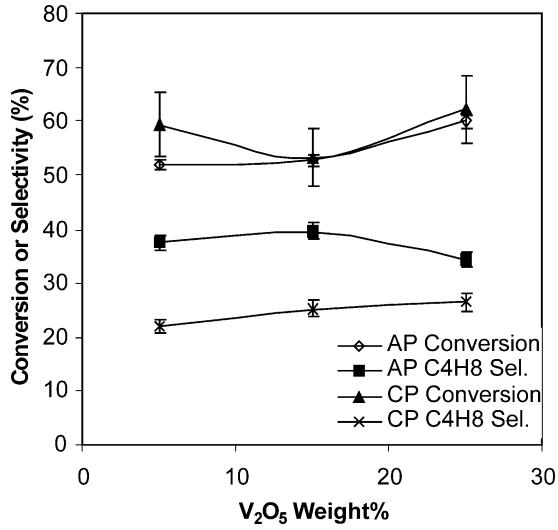

Fig. 8. Butane conversion and butene selectivity for AP and CP V/MgO with different V_2O_5 weight loadings.

Fig. 9 shows the CO and CO_2 selectivities and 95% confidence intervals for AP and CP V/MgO as functions of vanadium weight loading. For AP V/MgO CO selectivity

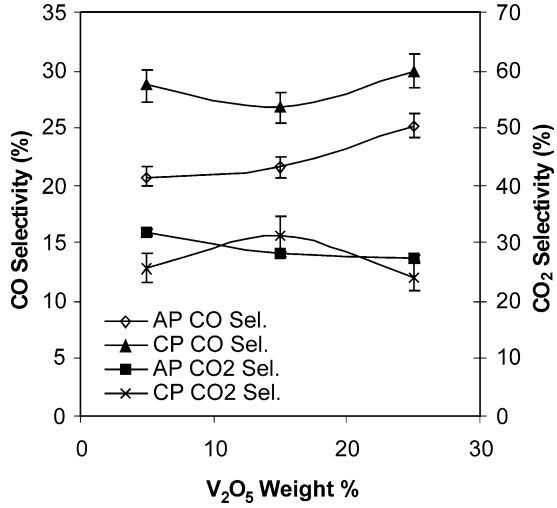

Fig. 9. CO and CO_2 selectivities for AP and CP V/MgO with different V_2O_5 weight loadings.

Table 3
Butane conversion and product selectivities for butane oxidative dehydrogenation over AP and CP V/MgO

	5 wt%		15 wt%		25 wt%	
	AP	CP	AP	CP	AP	CP
CH_4	0.4	0.7	0.4	0.2	0.5	1.0
CO	20.7	28.7	21.6	26.8	25.2	29.9
C_2H_6	0.1	0.2	0.1	0.1	0.2	0.2
CO_2	31.9	25.7	28.2	31.3	27.3	24.2
C_2H_4	6.6	16.7	6.8	11.9	8.7	13.1
C_3H_6	1.5	5.8	1.4	4.1	3.1	4.3
C_3H_8	0.0	0.0	0.4	0.0	0.0	0.0
C_4H_8	37.5	21.8	39.7	25.3	34.2	26.5
C_5H_{10}	1.3	0.4	1.3	0.5	0.9	0.8
Conversion	52.0	59.5	52.8	53.4	60.0	62.2

Experiments performed at a butane/oxygen ratio of 0.5 over 1 g of catalyst for a flow rate of 0.5 SLPM. All reported values are in %.

increases with weight loading from 21 to 25%. CO_2 selectivity, on the other hand, falls from 32 to 27%. For CP V/MgO, CO selectivity falls from 29 to 27% as weight loading increases from 5 to 15%, and then increases to 30% at a weight loading of 25%. CO_2 selectivitiy increases from 26 to 31% before falling to 24%. CO selectivity is higher on CP MgO than on AP MgO for all weight loadings. CO_2 selectivity is higher for CP V/MgO at a weight loading of 15%, while at weight loadings of 5 and 25%, CO_2 selectivity is higher on AP V/MgO. However, results at weight loadings of 15 and 25% are within experimental error.

Table 3 summarizes the catalytic results for all catalysts, including selectivities to minor products. In addition to the trend noted in Figs. 3 and 4, this table shows that CP V/MgO produces more ethylene and propylene than AP V/MgO.

4. Discussion

4.1. Catalyst structure

The XRD, Raman spectroscopy, XANES, and EXAFS results can aid in identifying the catalyst structure of all materials used in this study. Vanadium is likely present in small, isolated domains as evidenced by a lack of a diffraction pattern corresponding to vanadium phases. There is no evidence that V_2O_5 crystallites are present on any of the catalyst samples. The XANES and Raman results suggest that VO_x groups have a tetrahedral arrangement. Raman spectra suggest that primarily magnesium orthovanadate is present on all catalysts, especially at low loadings. However, there is likely magnesium pyrovanadate present for catalysts with weight loadings 15% and above, as shown by the broad band at $\sim$950 cm^{-1} for AP V/MgO at weight loadings of 15, 20, 25%, and 30% and for the CP V/MgO sample with 15 and 25 wt%.

XANES results provide evidence that increasing weight loading increases the amount of magnesium pyrovanadate present, as it was noted that the preedge peak width increased for both catalysts with weight loading. Increased width of this peak suggests broadening of the range of bond lengths, which would be expected if the amount of magnesium pyrovanadate increased. The narrowest width was noted for 5 wt% AP V/MgO, which Raman results suggested had only magnesium orthovanadate. It is interesting to note that the 5 wt% CP V/MgO had a broader preedge peak width than the AP V/MgO sample with the same weight loading. This could indicate that pyrovanadate was present on CP V/MgO at this weight loading while it was not present on AP V/MgO, although further proof is necessary to substantiate this.

It does not appear that there are significant differences in which the magnesium vanadate phase is present for AP and CP V/MgO, with the possible exception of the weight loading of 5%. For that weight percent, there are no discernible features in the CP V/MgO Raman spectrum, making it difficult to compare with the AP V/MgO spectrum. Ongoing analysis of the EXAFS spectra for all catalysts may provide more insight in the presence of the two magnesium vanadate phases for all weight loadings.

4.2. Catalytic differences

Significant catalytic differences were noted between the AP and CP catalysts. At a similar butane conversion, the selectivity to butene was higher on AP V/MgO, while CP V/MgO produced more CO, ethylene, and propylene. This was true at all weight loadings.

It is surprising that no butadiene was detected for any of the catalysts, since previous investigators have reported substantial butadiene selectivities, especially at high conversions [11,12,28,29]. It should be noted that the difference in the chromatograph retention times for butadiene and butene was only about half a minute. While no distinct butadiene peaks were noted, it is possible that small amounts of butadiene may have been obscured by the butene peak. It cannot, therefore, be concluded that these catalysts produced no butadiene. Rather, the butene selectivities reported should probably be interpreted as the total selectivity to dehydrogenation products, which might include small amounts of butadience.

Previous studies have explained catalytic differences based on the surface structure of vanadium. Blasco and coworkers [29] and others discuss how vanadium supported on basic supports generally gives higher oxidative dehydrogenation selectivity because of the presence of tetrahedral VO_4 units rather than acidic and nonselective V_2O_5 crystallites. Kung [30] proposed that the orthovanadate phase was more selective to butene than the pyrovanadate phase because the tetrahedral VO_4 units were isolated, thereby preventing overoxidation of butane. In this work, tetrahedral VO_4 groups are clearly present while V_2O_5 is absent; however, a substantial difference in the percentage of magnesium orthovanadate and pyrovanadate between AP and CP cata-

lysts has not been established. Magnesium orthovanadate appears to be the dominant species at all weight loadings for both AP and CP V/MgO. Therefore, the catalytic differences cannot be explained by differing amounts of the bulk magnesium vanadate phases.

This does not mean that catalyst structure could not be responsible for the observed catalytic differences. Bell and Iglesia have attributed activity and selectivity differences in oxidative dehydrogenation to the size of vanadate domains [31–33]. For vanadium supported on AP MgO, they proposed that the most active species for propane oxidative dehydrogenation are isolated domains of $Mg_3(VO_4)_2$ [8]. They suggested that these species are more selective than isolated VO_4^{2-} species and more active than bulk $Mg_3(VO_4)_2$. It is possible that the size of the $Mg_3(VO_4)_2$ domains differs between AP and CP V/MgO catalysts, and this difference is responsible for the observed catalytic trends. The catalyst characterization performed in this work is unable to resolve the domain size of $Mg_3(VO_4)_2$ phases, so there is no evidence with which to evaluate this theory.

Another theory is that the chemical nature of the supporting MgO is responsible for the catalytic differences between AP and CP V/MgO. If MgO plays a role in the oxidative dehydrogenation chemistry, then one would expect catalytic differences to result when the crystal size of the MgO support is changed. Several previous studies have suggested that MgO does play a role in oxidative dehydrogenation. Gao and co-workers reported higher propylene selectivity in propane oxidative dehydrogenation for Mg orthovanadate catalysts that contained some MgO than on pure magnesium orthovanadate [13]. Patel and co-workers found higher total dehydrogenation selectivity in the oxidative dehydrogenation of butane because of increased butadiene selectivity when a catalyst containing both magnesium orthovanadate and MgO phases was used instead of a pure magnesium orthovanadate phase [34]. Lemonidou and co-workers reported similar findings in the oxidative dehydrogenation of butane [28]. They proposed a cooperation between the two phases, specifically proposing that the presence of MgO induced a higher basicity on the surface of the catalyst, allowing alkenes to desorb easier and increasing olefin selectivity. This is essentially an argument that the acid/base nature of the catalyst affects oxidative dehydrogenation of alkanes [29,35].

It is known that AP MgO has significantly different chemical properties than CP MgO. Klabunde and co-workers have reported higher adsorption rates and capacities for AP MgO [10,36]. They have also reported different acid/base properties. Infrared spectroscopy studies found that surface OH groups of AP MgO were less acidic than OH groups on CP MgO [37]. In addition, more acid gases (SO_2 and CO_2) chemisorbed to AP MgO than CP MgO at the same partial pressure, suggesting a more efficient adsorption of acidic species [10]. This is consistent with the hypothesis that a more basic support can allow desorption of alkenes before they are oxidized to carbon oxides. It is also interesting to note that CP V/MgO has higher selectivity to cracking products ethylene and propylene. This is also consistent with higher basicity (lower acidity) for AP MgO, since higher acidity is known to increase cracking reactions.

A limited number of experiments were run using AP MgO and CP MgO as catalysts for butane oxidative dehydrogenation under the same conditions as used for V/MgO catalysts. While both MgO catalysts were not very selective to butene (selectivities under 3%), it was noted that AP MgO gave higher butene and CO_2 selectivities than CP MgO, while producing less CO and methane. These results suggest that AP MgO has different catalytic properties than CP MgO, and therefore the catalytic differences noted for AP V/MgO and CP V/MgO could be due to the unique properties of the supports.

5. Conclusions

Vanadium supported on AP MgO provides very different catalytic behavior than vanadium supported on CP MgO. At a similar butane conversion, selectivity to butene was higher on AP V/MgO, while CO, ethylene, and propylene selectivities were all lower, irrespective of V_2O_5 weight loading. The catalyst surface structure on AP and CP MgO appears to be similar, with an magnesium orthovanadate phase supported on a MgO phase. At higher weight loadings, magnesium pyrovanadate may also be present. It is hypothesized that differences in the surface chemistry of AP MgO and CP MgO are responsible for the catalytic differences, though differences in the domain size of $Mg_3(VO_4)_2$ could also play a role. Higher basicity of AP MgO may allow faster desorption of butene during oxidative dehydrogenation, leading to the higher butene selectivity noted for AP V/MgO.

Acknowledgments

The authors acknowledge Klaus Attenkofer, Jennifer Linton, and Randall Winans at BESSRC-CAT at Argonne National Laboratories for assistance in obtaining all XANES results. The authors also acknowledge the contributions of Nathan Fritz, who was supported by ACS Project SEED, in preparing the AP V/MgO catalysts used in this work. This work was supported by DOE EPSCOR Grant DE-FG02-01ER45896.

References

[1] A. Tschope, J.Y. Ying, in: G.C. Hadjipanayis, R.W. Siegel (Eds.), Nanophase Materials: Synthesis–Properties–Applications, Kluwer Academic, Dordrecht, The Netherlands, 1994, p. 781.
[2] Z. Zhang, C.-C. Wang, R. Zakaria, J.Y. Ying, J. Phys. Chem. B 102 (1998) 10871.
[3] A.J. Maira, K.L. Yeung, C.Y. Lee, P.L. Yue, C.K. Chan, J. Catal. 192 (2000) 185.

[4] K.Y. Jung, S. Bin Park, S.K. Ihm, Appl. Catal. A 224 (2002) 229.
[5] A.E.C. Palmqvist, E.M. Johansson, S.G. Jaras, M. Muhammed, Catal. Lett. 56 (1998) 69.
[6] A.E.C. Palmqvist, M.F.M. Zwinkels, Y. Zhang, S.G. Jaras, M. Muhammed, Nanostruct. Mater. 8 (1997) 801.
[7] J.S. Yoo, Catal. Today 41 (1998) 409.
[8] C. Pak, A.T. Bell, T.D. Tilley, J. Catal. 206 (2002) 49.
[9] V.V. Chesnokov, A.F. Bedilo, D.S. Heroux, I.V. Mishakov, K.J. Klabunde, J. Catal., in press.
[10] K.J. Klabunde, J. Stark, O. Koper, C. Mohs, D.G. Park, S. Decker, Y. Jiang, I. Lagadic, D. Zhang, J. Phys. Chem. 100 (1996) 12142.
[11] M.A. Chaar, D. Patel, M.C. Kung, H.H. Kung, J. Catal. 105 (1987) 483.
[12] J.M. Lopez Nieto, A. Dejoz, M.I. Vazquez, W. O'Leary, J. Cunningham, Catal. Today 40 (1998) 215.
[13] X. Gao, P. Ruiz, Q. Xin, X. Guo, B. Delmon, J. Catal. 148 (1994) 56.
[14] C. Tellez, M. Abon, J.A. Dalmon, C. Mirodatos, J. Santamaria, J. Catal. 195 (2000) 113.
[15] J. Hanuza, B. Jezowska-Trzebiatowska, W. Oganowski, J. Mol. Catal. 29 (1985) 109.
[16] G. Busca, G. Ricchiardi, D.S.H. Sam, J.-C. Volta, J. Chem. Soc., Faraday Trans. 90 (1994) 1161.
[17] A. Khodakov, B. Olthof, A.T. Bell, E. Iglesia, J. Catal. 181 (1999) 205.
[18] J. Wong, F.W. Lytle, R.P. Messmer, D.H. Maylotte, Phys. Rev. B 30 (1984) 5596.
[19] T. Tanaka, H. Yamashita, R. Tsuchitani, T. Funabiki, S. Yoshida, J. Chem. Soc., Faraday Trans. 1 84 (1988) 2987.
[20] H.T. Evans Jr., Z. Krystallogr. Mineral. 114 (1960) 257.
[21] D.S.H. Sam, V. Soenen, J.C. Volta, J. Catal. 123 (1990) 417.
[22] N. Krishnamachari, C. Calvo, Can. J. Chem. 49 (1971) 1629.
[23] P. Cramer, K.O. Hodgson, E.I. Stiefel, W.E. Newton, J. Am. Chem. Soc. 100 (1978) 2748.
[24] M. Nabavi, F. Taulelle, C. Sanchez, M. Verdaguer, J. Phys. Chem. Solids 51 (1990) 1375.
[25] X. Gao, S.R. Bare, B.M. Weckhuysen, I.E. Wachs, J. Phys. Chem. B 102 (1998) 10842.
[26] S. Takenaka, T. Tanaka, T. Yamazaki, T. Funabiki, S. Yoshida, J. Phys. Chem. B 101 (1997) 9035.
[27] K. Inumaru, T. Okuhara, M. Misono, N. Matsubayashi, H. Shimada, A. Nishijima, J. Chem. Soc., Faraday Trans. 88 (1992) 625.
[28] A.A. Lemonidou, G.J. Tjatjopoulos, I.A. Vasalos, Catal. Today 45 (1998) 65.
[29] T. Blasco, J.M. Lopez Nieto, Appl. Catal. A 157 (1997) 117.
[30] H.H. Kung, M.C. Kung, Appl. Catal. A 157 (1997) 105.
[31] A. Khodakov, B. Olthof, A.T. Bell, E. Iglesia, J. Catal. 181 (1999) 205.
[32] A. Khodakov, J. Yang, S. Su, E. Iglesia, A.T. Bell, J. Catal. 177 (1998) 343.
[33] K. Chen, A.T. Bell, E. Iglesia, J. Catal. 209 (2002) 35.
[34] D. Patel, P.J. Anderson, H.H. Kung, J. Catal. 125 (1990) 132.
[35] S. Albonetti, F. Cavani, F. Trifiro, Catal. Rev.-Sci. Eng. 38 (1996) 413.
[36] Y. Jiang, S. Decker, C. Mohs, K.J. Klabunde, J. Catal. 180 (1998) 24.
[37] H. Itoh, S. Utamapanya, J.V. Stark, K.J. Klabunde, J.R. Schlup, Chem. Mater. 5 (1993) 71.